Thomas Veltzke, Lars Kiewidt and Jorg Thöming

Multicomponent gas diffusion in nonuniform tubes

Journal Article as: peer-reviewed accepted version (Postprint)

DOI of this document*(secondary publication): 10.26092/elib/2454

Publication date of this document: 08/09/2023

Recommended Citation (primary publication/Version of Record) incl. DOI:

Thomas Veltzke, Lars Kiewidt and Jorg Thöming
Multicomponent gas diffusion in nonuniform tubes
AIChE journal, Volume 61, Issue 4, 2015, pages 1404-1412, ISSN 0001-1541
https://doi.org/10.1002/aic.14711

Multicomponent Gas Diffusion in Nonuniform Tubes

Thomas Veltzke, Lars Kiewidt, and Jorg Thöming
Dept. of Chemical Engineering, Center for Environmental Research and Sustainable Technology (UFT), University of Bremen, 28359 Bremen, Germany

DOI 10.1002/aic.14711
Published online December 26, 2014

In many technical processes gas, multicomponent diffusion takes place in confinements that are rarely uniform in direction of their long axis (e.g., catalysts pores). Here, we show that in conical tubes multicomponent diffusion is hindered. This effect increases with ratio of inlet to outlet cone radius Λ, indifferent of the orientation of the tube. Based on the Maxwell–Stefan equations, predictive analytical solution for ideal multicomponent diffusion in slightly tapered ducts is developed. In two-bulb diffusion experiments on a uniform tube, the results of Duncan and Toor (1962) were reproduced. Comparison of model and experiment shows that the solution presented here provides a reliable quantitative prediction of the temporal change of H_2, N_2, and CO_2-concentration for both tube geometries, uniform and slightly conical. In the demonstrated case ($\Lambda = 3.16$), mass diffusion is 68% delayed. Thus, for gaseous diffusion in "real," typically tapered pores the transport limitation is more serious than considered so far. © 2014 American Institute of Chemical Engineers *AIChE J*, 61: 1404–1412, 2015

Keywords: gas multicomponent diffusion, experiments on conical tubes, classical Maxwell–Stefan equations, analytical transport model, two-bulb diffusion experiment

Introduction

Multicomponent diffusion is a crucial transport mechanism that determines the integral behavior and efficiency of many natural and technical processes such as mixed gas separation using porous membranes, fuel cells, and heterogeneous catalysis. Being aware of the variety of mechanisms discussed in literature, only bulk diffusion in gases is considered in this work. For a more comprehensive overview of transport mechanisms, reference is made to the books of Bird et al.[1] and Taylor and Krishna.[2] For the modeling of gaseous diffusion with superimposed pressure-driven flows and under presence of a liquid phase, we refer to the work of Zhukovsky et al.[3–6]

A common approach to describe molecular diffusion is Fick's first law,[7,8] which states that the molar flux in a mixture is proportional to its concentration gradient and directed against it. Hence, no influence of the other components is considered meaning that multicomponent-effects are ignored. Actually, such multicomponent-effects can completely divert the diffusive fluxes, leading to so-called reverse diffusion (up-hill diffusion in direction of the gradient), osmotic diffusion (diffusion without a concentration gradient of the targeting component), and diffusion barrier (no diffusion despite a gradient).[2,9,10] Hence, Fick's approach is strictly limited to single gases and binary mixtures which was shown experimentally by Duncan and Toor[11] who investigated diffusion in ideal ternary gas mixtures by means of the two-bulb diffusion experiment. Physically osmotic diffusion, reverse diffusion, and the diffusion barrier can be explained qualitatively with intermolecular friction forces. As Maxwell[12] and Stefan[13] already discovered in the 19th century, a more general approach that accounts for the intermolecular friction is required to describe diffusion in multicomponent systems. This approach, often referred as classical Maxwell–Stefan equations (MSE), has been successfully used by several scientists and engineers like, among others, Bird et al.,[1] Krishna and Wesselingh,[9] Lightfoot,[14] Krishna and Standart,[15] and Kapteijn et al.[16] to predict multicomponent transport such as in the two-bulb diffusion experiment of Duncan and Toor.[11]

In current literature, experimental and numerical analysis on multicomponent diffusion confine solely on uniform ducts as object of examination. This is wondrous as "real" confinements in which diffusion takes place (e.g., pores, microelectromechanical systems) typically are somehow tapered (see Figure 1), and diffusive flow can significantly depend on the gradient of the duct's cross-sectional area as we could show for pressure-driven flows by an own earlier work.[17] In such flows, a gas flow diode effect was observed experimentally,[17,18] numerically,[19] and analytically[17,19] meaning that a tapered duct has a preferred direction of perfusion when the gas is in a rarefied state.

Thus, the urgent questions that arise here are: how will multicomponent diffusion be affected by conicity of the tube that connects the bulbs in the two-bulb diffusion experiment? And, do effects occur that are analogous to the gas flow diode effect in pressure-driven rarefied gas flows? These questions are analytically and experimentally investigated in this work.

In the following section, we present an analytical model based on the work of Duncan and Toor[11] to describe multicomponent diffusion in slightly tapered geometries.

Correspondence concerning this article should be addressed to T. Veltzke at tveltzke@uni-bremen.de.

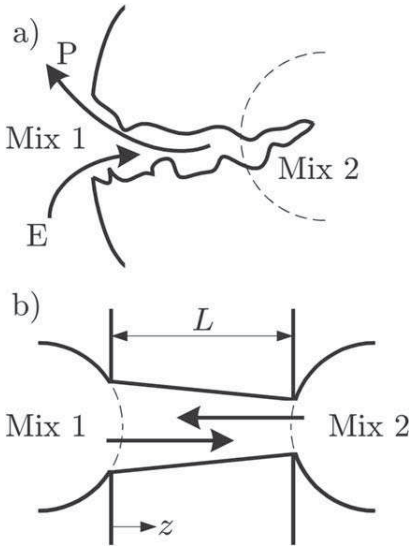

Figure 1. Idealized catalyst pore as an example of a "real" pore (a). Educts *E* enter the pore and react to products *P* which leave the pore. Diffusion is the only transport mechanism because of the absence of a pressure gradient. In (b), the situation is simplified. The abstraction results in the schematic of the two-bulb diffusion cell with a tapered duct.

Subsequently, in Section Experimental, the experimental setup is described. Finally, we compare our theoretical and experimental findings in Section Results, and conclude with an interpretation of our results regarding future applications in Section Conclusions.

Model Development and Theoretical Analysis

Let us consider two bulbs containing gas mixtures with n species i that are connected by a long duct of alongside variable cross section. In Figure 1b that setup is illustrated as an abstraction of an idealized catalyst pore where the concentration varies from the educt-rich bulk to the product-rich end of the pore.

The temperature in both bulbs is identical and the overall system is isothermal. We define z as the longitudinal coordinate in the flow direction with the origin in the first reservoir at $z = 0$. According to Figure 1b, the length of the duct is L and the (arbitrary) cross section is $A(z)$. Correspondingly, the left bulb of the experiment is in the following indicated by superscript (0) whereas the right bulb is indicated by superscript (L). The volumes V of both reservoirs are identical.

Bulb species balance

Beginning with an integral species balance around each bulb we write

$$\frac{\partial}{\partial t}\int_{(V)} c_i^{(0)}\,dV = -\int_{(A^{(0)})} \mathbf{J}_i^{(0)}\cdot\mathbf{n}\,dA^{(0)} \tag{1a}$$

$$\frac{\partial}{\partial t}\int_{(V)} c_i^{(L)}\,dV = +\int_{(A^{(L)})} \mathbf{J}_i^{(L)}\cdot\mathbf{n}\,dA^{(L)} \tag{1b}$$

where c_i and $\mathbf{J}_i$ are the concentration of species i and its diffusive flux counted positive in the positive z-direction, respectively. Here, we assume that the gas mixture in each bulb is well mixed and thus spatial concentration variations are negligible. Further, we assume that the diffusive fluxes are homogeneously distributed over the cross section of the connecting tube. Consequently, performing the integrals in (1a) and (1b) yields

$$V\frac{\partial c_i^{(0)}}{\partial t} = -\mathbf{J}_i^{(0)}A^{(0)} \tag{2a}$$

$$V\frac{\partial c_i^{(L)}}{\partial t} = +\mathbf{J}_i^{(L)}A^{(L)} \tag{2b}$$

The gas mixture is treated as an ideal gas at constant pressure and temperature, and chemical reactions are neglected so that the total concentration in both bulbs $c_t = p/(RT) = c_i/x_i$ remains constant over time. Furthermore, as we are dealing with a closed system, the number of moles of each species in the whole system has to be constant at any instant in time. Thus, the overall species balance around both bulbs, neglecting the small volume of the connecting tube, reads

$$2c_i^{(\mathrm{eq})} = c_i^{(0)} + c_i^{(L)} \tag{3}$$

Equation 3 allows us to treat the bulbs separately because the composition in one bulb can easily be computed from the composition in the other bulb and the known equilibrium composition. The latter is the arithmetic average of the initial composition in both bulbs. Here, we focus on the left bulb; the derivation for the right bulb (index L) is analogous and therefore not stated here explicitly.

Considering the isobaric, isothermal, and nonreacting conditions Eq. 1ba reads

$$c_t V\frac{\partial x_i^{(0)}}{\partial t} = \mathbf{J}_i^{(0)}A^{(0)} \tag{4}$$

where $x_i^{(0)}$ are the mole fractions in the left bulb. To compute the diffusive fluxes, $\mathbf{J}_i$, we use the MSE

$$\frac{dx_i^{(0)}}{dz} = -\sum_{\substack{j=1\\ j\neq i}}^{n}\frac{x_i^{(0)}x_j^{(0)}}{Đ_{ij}}\left(\mathbf{u}_i-\mathbf{u}_j\right) = \sum_{\substack{j=1\\ j\neq i}}^{n}\frac{x_i^{(0)}\mathbf{J}_j^{(0)} - x_j^{(0)}\mathbf{J}_i^{(0)}}{c_t Đ_{ij}} \tag{5}$$

where $Đ_{ij}$ are the Maxwell–Stefan diffusivities estimated by the Chapman–Enskog kinetic theory [Ref. 1, p. 526]. As we assume the fluxes to be constant over the cross section, we write the gradients only in the z-direction. An explicit expression for the diffusive fluxes, $\mathbf{J}_i^{(0)}$, can be obtained by inverting Eq. 5 using the relation

$$\sum_{i=1}^{n} x_i^{(0)} = 1 \quad \text{or equivalently} \quad \sum_{i=1}^{n}\frac{dx_i^{(0)}}{dz} = 0 \tag{6}$$

to obtain

$$\mathbf{J}_i^{(0)} = -c_t\sum_{j=1}^{n-1} D_{ij}\frac{dx_j^{(0)}}{dz} \tag{7}$$

Here, D_{ii} are the Fickian diffusivities, that is, diffusive transport of species i due to a concentration gradient of species i, whereas D_{ij} $(i \neq j)$ are the cross diffusivities describing multicomponent effects. The matrix of diffusivities is defined as

$$[D]=[B]^{-1} \tag{8}$$

where

$$\begin{aligned} B_{ii} &= \frac{x_i}{Đ_{in}} + \sum_{\substack{j=1 \\ j\neq i}}^{n} \frac{x_j}{Đ_{ij}} \\ B_{ij} &= -x_i\left(\frac{1}{Đ_{ij}} - \frac{1}{Đ_{in}}\right) \end{aligned} \tag{9}$$

It should be noted that the diffusivities in Eq. 7 depend on the composition of the mixture and may also take negative values to account for multicomponent effects.

Inserting the inverted MSE into Eq. 4 yields

$$\frac{\partial x_i^{(0)}}{\partial t} = -\frac{A^{(0)}}{V}\sum_{j=1}^{n-1} D_{ij}\frac{dx_j^{(0)}}{dz} \tag{10}$$

Equation 10, together with Eqs. 3 and 6, describe the temporal change of the molar fractions in both bulbs including multicomponent effects.

The solution of Eq. 10, however, requires the knowledge of the spatial concentration gradients within the connecting duct that will be analyzed in the following.

Duct species balance

To obtain the spatial gradients of the molar fraction of each species at the bulb inlets, the spatial composition profiles within the duct, $x_i(z)$, require closer examination. So far, the model is identical to the one of Duncan and Toor.[11] In their work, they assumed a linear profile of the molar fractions and thus a constant gradient at both ends of the duct. This, however, is invalid for the scenario of tapered geometries considered here.

Following Fick,[8] we consider an incremental section of the tapered duct shown in Figure 2. The species balances for the incremental duct section read

$$c_t A\delta z\frac{\partial x_i}{\partial t} = \mathbf{J}_i^- A^- - \mathbf{J}_i^+ A^+ \tag{11}$$

Using truncated Taylor series to describe the influxes and outfluxes

$$\mathbf{J}_i^- A^- = \mathbf{J}_i A - \frac{\delta z}{2}\frac{d}{dz}(\mathbf{J}A) \tag{12a}$$

$$\mathbf{J}_i^+ A^+ = \mathbf{J}_i A + \frac{\delta z}{2}\frac{d}{dz}(\mathbf{J}A) \tag{12b}$$

and substituting Eq. 10 into Eq. 11 yields

$$c_t A\delta z\frac{\partial x_i}{\partial t} = -\frac{d}{dz}(\mathbf{J}_i A)\delta z \tag{13}$$

Next, we apply the chain rule to the right-hand side of Eq. 13 and divide by $A\delta z$ to get

$$c_t\frac{\partial x_i}{\partial t} = -\frac{dJ_i}{dz} - \mathbf{J}_i\frac{1}{A}\frac{dA}{dz} \tag{14}$$

At this point of the derivation, it is useful to have a closer look at the time scales associated with the bulbs and the duct. By choosing a characteristic mole fraction x_c and diffusive flux $\mathbf{J}_c$, we obtain the following characteristic time for a composition change to happen at the bulb scale from Eq. 4

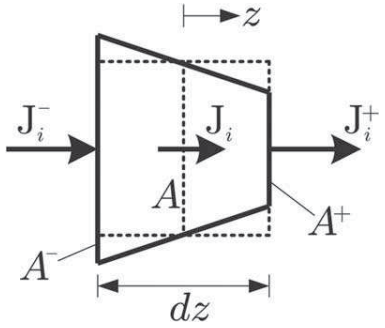

Figure 2. Increment of a slightly tapered tube.

$$t_c^{(\mathrm{b})} = \frac{p}{RT}\frac{V}{A}\frac{x_c}{\mathbf{J}_c} \tag{15}$$

The constant total concentration c_t is expressed by temperature and pressure via the ideal gas relation.

For the duct scale, we apply the same characteristic mole fraction and diffusive flux, and choose the duct length L as characteristic length for the coordinate z. Using Eq. 14, then yields the characteristic time for composition changes to happen at the duct scale

$$t_c^{(\mathrm{d})} = \frac{p}{RT}L\frac{x_c}{\mathbf{J}_c} \tag{16}$$

Comparing both time scales finally yields

$$\frac{t_c^{(\mathrm{d})}}{t_c^{(\mathrm{b})}} = \frac{AL}{V} \tag{17}$$

This means that, if the volume of a single bulb is much larger than the volume of the duct, we can safely neglect transient changes within the duct at the bulb scale. Consequently, we can treat the duct as quasistationary and omit the left-hand side of Eq. 14 to obtain

$$\frac{dJ_i}{dz} + \mathbf{J}_i\frac{1}{A}\frac{dA}{dz} = 0 \tag{18}$$

Again, using the MSE (5) to compute the diffusive fluxes gives

$$\frac{d}{dz}\left(\sum_{j=1}^{n-1} D_{ij}\frac{dx_j}{dz}\right) + \frac{1}{A}\frac{dA}{dz}\sum_{j=1}^{n-1} D_{ij}\frac{dx_j}{dz} = 0 \tag{19}$$

Now, we assume that the diffusivities are constant to get the steady-state Fick–Jacobs equation[8,20]

$$\frac{d^2x_i}{dz} + \frac{1}{A}\frac{dA}{dz}\frac{dx_i}{dz} = 0 \tag{20}$$

Formally, this is equivalent to multiplying Eq. 19 with the inverse of the diffusivity matrix. The assumption of constant diffusivities is generally not true because they change with composition, however, it allows an analytical solution. Later, we will revisit this assumption and check its validity.

As stated by Zwanzig[21] and Berezhkovskii,[22] the Fick–Jacobs equation is only valid for slightly tapered cross sections. In the following, we assume the duct as a conical tube with slightly varying radius $r(z)$. Let the slight inclination $m=(r^{(L)}-r^{(0)})/L$ be constant with boundary values $r(z=0)=r^{(0)}$ and $r(z=L)=r^{(L)}$. Using these definitions, we obtain

$$A(z)=\pi(r^{(0)}+mz),\quad \frac{dA}{dz}=2\pi m(r^{(0)}+mz),\quad \frac{1}{A}\frac{dA}{dz}=\frac{2m}{r^{(0)}+mz} \tag{21}$$

Now, we substitute dx_i/dz in Eq. 20 by s and by applying the expressions stated in Eq. 21, we obtain

$$\frac{ds}{dz}=\frac{2m}{r^{(0)}+mz}s \tag{22}$$

Integration yields

$$\begin{aligned}&\ln s=-2\ln\left(r^{(0)}+mz\right)+a\\ &\Rightarrow s=\frac{C_1}{\left(r^{(0)}+mz\right)^2};\quad C_1=e^a\end{aligned} \tag{23}$$

Replacing s again by dx_i/dz and integrating a second time, we obtain

$$x_i=-\frac{C_1}{m(r^{(0)}+mz)}+C_2 \tag{24}$$

By means of the transient boundary conditions

$$x_i(z=0,t)=x_i^{(0)}(t),\quad x_i(z=L,t)=x_i^{(L)}(t) \tag{25}$$

we determine the integration constants

$$x_i(z=0,t)=x_i^{(0)}(t)=-\frac{C_1}{mr^{(0)}}+C_2 \tag{26a}$$

$$x_i(z=L,t)=x_i^{(L)}(t)=-\frac{C_1}{m(r^{(0)}+mL)}+C_2=-\frac{C_1}{mr^{(L)}}+C_2 \tag{26b}$$

From Eq. 26a

$$C_2=x_i^{(0)}(t)+\frac{C_1}{mr^{(0)}} \tag{27}$$

Inserting Eq. 27 in Eq. 26b yields

$$\begin{aligned}&x_i^{(L)}(t)=-\frac{C_1}{mr^{(L)}}+x_i^{(0)}(t)+\frac{C_1}{mr^{(0)}}\\ &\Rightarrow x_i^{(L)}(t)-x_i^{(0)}(t)=\frac{r^{(L)}-r^{(0)}}{mr^{(L)}r^{(0)}}C_1\\ &\Rightarrow C_1=\frac{mr^{(0)}}{1-\Lambda}\left(x_i^{(L)}(t)-x_i^{(0)}(t)\right)\end{aligned} \tag{28}$$

with Λ being the ratio of $r^{(0)}$ to $r^{(L)}$ (i.e., is unity for a uniform duct). Hence, C_2 writes

$$C_2=x_i^{(0)}(t)+\frac{1}{1-\Lambda}\left(x_i^{(L)}(t)-x_i^{(0)}(t)\right) \tag{29}$$

Applying both integration constants to Eq. 24, one obtains

$$x_i(t)=x_i^{(0)}(t)+\left(x_i^{(L)}(t)-x_i^{(0)}(t)\right)\left(\frac{z}{L\Lambda+(1-\Lambda)z}\right) \tag{30}$$

Differentiation of Eq. 30 yields

$$\frac{dx_i}{dz}(t)=\frac{L\Lambda}{(L\Lambda-\Lambda z+z)^2}\left(x_i^{(L)}(t)-x_i^{(0)}(t)\right) \tag{31}$$

and we obtain the required gradient in Eq. 10 as

$$\left.\frac{dx_i}{dz}\right|_{z=0}(t)=\frac{1}{\Lambda}\frac{x_i^{(L)}(t)-x_i^{(0)}(t)}{L} \tag{32}$$

The problem that arises here is that $dx_i^{(0)}/dz$ is a function of the molar fractions in the right bulb at $z=L$. To eliminate $x_i^{(L)}$ from Eq. 32, we make use of the component material balance around both bulbs, Eq. 3, as also presented in literature.[2]

Combining now Eqs. 3, 6, and 10 with (32), where index i is adjusted according to Eq. 10, yields $n-1$ first-order ordinary differential equations in time and $n+1$ algebraic equations

$$\frac{dx_i^{(0)}(t)}{dt}=-\frac{1}{\Lambda}\frac{2A^{(0)}}{VL}\sum_{j=1}^{n-1}D_{ij}\left(x_j^{\infty}-x_j^{(0)}(t)\right),\quad i=1,\ldots,n-1 \tag{33a}$$

$$x_n^{(0)}(t)=1-\sum_{i=1}^{n-1}x_i^{(0)}(t) \tag{33b}$$

$$x_i^{(L)}(t)=2x_i^{\infty}-x_i^{(0)}(t),\quad i=1,\ldots,n \tag{33c}$$

Given the initial conditions $x_i^{(0)}(t=0)=x_{i,t^*}^{(0)}$, Eqs. 33a–33c fully specify the dynamic behavior of the molar fractions in both bulbs connected by a slightly conical tube. The special case of a binary mixture ($n=2$) is also included in Eqs. 33a–33c.

Model solution and analysis

Equations 33 are coupled by the cross diffusivities. An analytical solution, however, is possible using linearized theory based on eigenvalue decomposition[2] because of the assumption of constant diffusivities. The analytical solution of Eq. 33a reads in the eigenvalue space

$$\hat{x}_i^{(0)}=\left(\hat{x}_{i,t^*}^{(0)}-\hat{x}_i^{\infty}\right)\exp\left(-\frac{1}{\Lambda}\frac{2A^{(0)}}{LV}\hat{D}_i t\right)+\hat{x}_i^{\infty} \tag{34}$$

where $\hat{D}_i$ are the eigenvalues of the diffusivity matrix

$$[\hat{D}]=[P]^{-1}[D][P] \tag{35}$$

and $\hat{x}_i$ are the so-called pseudocompositions in the eigenvalue space

$$(\hat{x})=[P]^{-1}(x). \tag{36}$$

The matrix $[P]$ contains the eigenvectors of the diffusivity matrix. After computing the pseudocompositions, $\hat{x}_i$, from Eq. 34 the physical compositions are calculated using

$$(x)=[P](\hat{x}) \tag{37}$$

and Eqs. 33b and 33c. The eigenvalues and eigenvectors of the diffusivity matrix can easily be computed using standard linear algebra routines in MATLAB.

By means of Eq. 34, we can expect that diffusion is delayed in conical tubes and that the time τ to reach a certain molar fraction is minimum in case of a uniform geometry, respectively. Using Eq. 34, we equate the molar fraction in the case of the conical tube with the molar fraction in the case of the uniform tube

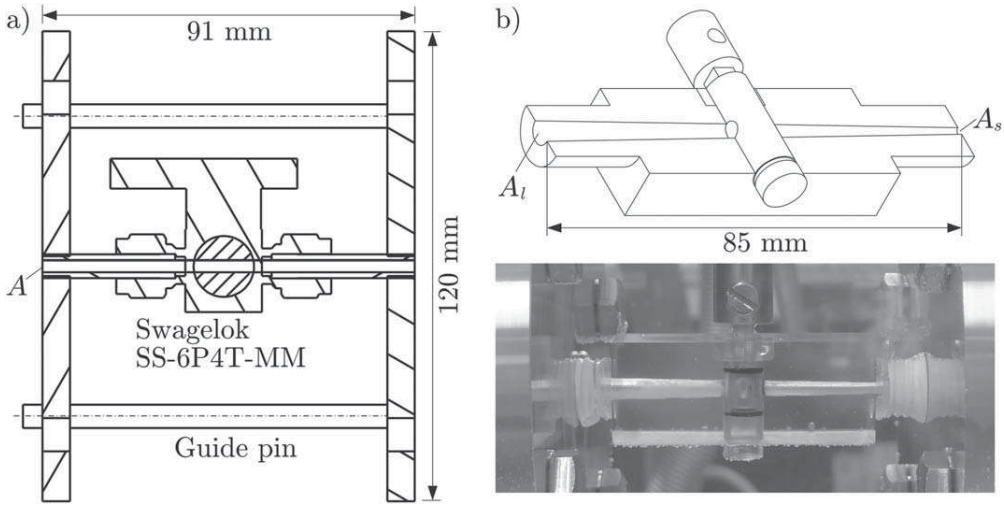

Figure 3. Test tubes used in experiments: with uniform cross section (a) and slightly conical (b).

All dimensions of both tubes are stated in Table 1.

$$\exp\left(-\frac{1}{\Lambda}\frac{2A^{(0)}}{L_{\text{cone}}V}\hat{D}_i\tau_{\text{cone}}\right)=\exp\left(-\frac{2A}{L_{\text{uni}}V}\hat{D}_i\tau_{\text{uni}}\right)$$
$$\Rightarrow \tau_{\text{cone}}=\alpha\tau_{\text{uni}} \quad \text{with} \quad \alpha=\Lambda\frac{AL_{\text{cone}}}{A^{(0)}L_{\text{uni}}} \tag{38}$$

When the assumption is made that the uniform tube and the conical tube have identical average cross section $A=\bar{A}=0.5\pi(r_s^2+r_l^2)$ and length, we find for the hindrance factor

$$\alpha=\frac{\left(r^{(0)}\right)^2+\left(r^{(L)}\right)^2}{2r^{(0)}r^{(L)}}>1 \quad \text{for} \quad A=\bar{A};L_{\text{cone}}=L_{\text{uni}} \tag{39}$$

Consequently, diffusion is delayed in tapered ducts by the hindrance factor α that, for a slightly conical tube, is a constant value depending solely on the disparity of $r^{(0)}$ and $r^{(L)}$. As if can be seen by Eq. 39, it is indifferent whether $r^{(0)}$ or $r^{(L)}$ is larger, meaning that the diffusion hindrance does not depend on the direction of the cone (converging or diverging along z).

The derived model is used for the prediction of the temporal change of the molar fractions of a ternary gas mixture in the two-bulb diffusion experiment. The experimental conditions and details on the setup are given in the following.

Experimental

Test tubes

The two-bulb diffusion experiments were performed with two different tube geometries. The first one is a uniform tube as used by Duncan and Toor[11] for benchmarking reasons. A sectional drawing of this uniform tube with integrated stopcock is shown in Figure 3a. The two single tubes with a nominal inner diameter of 3.4 mm and the stopcock (SS-6P4T-MM) are commercially available from Swagelok that are assembled between custom-made flanges. All components are made of stainless steel and the connections to the flanges are welded. The second tube has a linearly changing radius and is produced by stereo-lithography by tobaTEC GmbH, Germany. According to Figure 3b, the tube is a conical hole in a block and a rotatable cylinder acts as a stopcock. Both parts are made of acrylonitrile butadiene styrene and are sealed with vacuum grease.

The length L of both tubes is measured 10 times with a digital caliper and the mean and the uncertainty are calculated. The small and large cross sections are measured with digital light microscopy (pictures are provided in Appendix, Figure A1) and small and large radius were derived as

$$r_s=\sqrt{\frac{A_{s,\text{measured}}}{\pi}}; \quad r_l=\sqrt{\frac{A_{l,\text{measured}}}{\pi}} \tag{40}$$

The determined dimensions are stated in Table 1.

Experimental setup and procedure

According to Figure 4, the experimental setup consists of two bulbs that are connected by one of the previously described test channels. The bulbs are made of stainless steel and the volumes are given in Table 1. Each volume was determined three times (for calculation of mean and uncertainty) by filling in water and measuring the difference in weight of the empty and filled bulb. Dividing by the density of water (994.6 kg m^{-3} at 296.7 K) yields the bulb volume of approximately 340 cm^3. The dimensions of test tubes and bulbs justify the assumption according to Eq. 17. Using the values given in Table 1, we find that composition changes happen approximately 400 times as fast in the duct as in the bulbs.

Table 1. Experimental Dimensions

	Symbol	Dimension
Volume Bulb A	V_A	340.89 ± 0.45 cm^3
Volume Bulb B	V_B	339.11 ± 1.35 cm^3
Uniform tube		
Length	L	91.01 ± 0.02 mm
Cross section	A	9.250 mm^2
Radius	r	1.716 mm
Conical tube		
Length	L	84.98 ± 0.03 mm
Small cross section	A_s	1.626 mm^2
Large cross section	A_l	16.246 mm^2
Average cross section	$\bar{A}=0.5(A_s+A_l)$	8.936 mm^2
Small radius	r_s	0.719 mm
Large radius	r_l	2.274 mm
Radius ratio	$\Lambda=r_l/r_s$	3.16

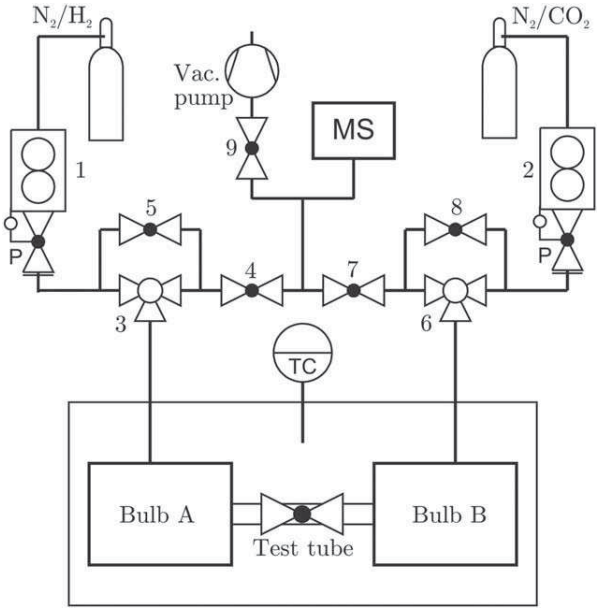

Figure 4. Apparatus used for the two-bulb diffusion experiments.

The different tubes (Figure 3, Table 1) with integrated stopcock can be implemented between bulbs A and B made of stainless steel. The apparatus is shown embedded in the process flow diagram.

Bulbs and test tube are placed in a water bath ($\approx$ 0.04 m^3) with controlled temperature (always 308.15 K in reference to Duncan and Toor[11]). Concerning the valves and other periphery the apparatus is strictly symmetric.

The experimental procedure was as follows. The left part is evacuated with the vacuum pump (valve 7 is closed while valves 3, 4, 5, and 9 are open) and the mass spectrometer (GAM200, InProcessInstruments mbH, Germany) was running for monitoring purpose. Then, valve 9 was closed and the N_2/H_2 gas mixture (6.0 quality, Linde AG, Germany) was filled in via pressure controller 1 until approximately 0.1 MPa(a) was reached. Afterward, valve 9 was opened again and the procedure was repeated three times to assure that residues of the previous experiment are negligible. This was successfully proved by the mass spectrometer showing a N_2 concentration of 0.5012, a H_2 concentration of 0.4978, and the concentration of CO_2 as negligible. Those values are taken as initial concentrations for the calculations (see Table A3 in Appendix). Finally, the pressure was adjusted to exactly 0.1 MPa(a) and valve 4 was closed. The very same procedure was done for the right part where a N_2 concentration of 0.5016, a CO_2 concentration of 0.4963, and a negligible H_2 concentration was measured. After waiting 20 min to assure that the gas mixtures in both bulbs are at constant temperature, the three-way valves 3 and 6 were closed and the integrated stopcock of the test tube was opened to start the experiment.

The stopcock was shut again after a designated time (see Tables A1–A3 in Appendix) to finish and to analyze the experiment. Therefore, in case of bulb A, valves 3, 5, and 7 were closed and valves 4 and 9 were opened to evacuate the tubes. Then, valve 9 was closed and valve 3 was opened toward the mass spectrometer and the composition was analyzed. The same was done for bulb B using the corresponding valves. The procedure was repeated for a range of times up to 40 h to evaluate the temporal behavior of the diffusion experiments.

The conical tube (Figure 3b) was assembled twofold between bulb A and B: diverging along the z-coordinate (Figure 5b) and in converging direction (Figure 5c).

Results

Preceding calculations

For the predictive calculation of the temporal change of the molar fraction of each three species in the bulbs, the diffusivities (see Eq. 33a) are required. As mentioned in Section Model Development and Theoretical Analysis, the binary diffusivities can be estimated according the Chapman–Enskog kinetic theory [Ref. 1, p. 526]. For 308.15 K and 0.1 MPa(a), one obtains $D_{N_2/CO_2}=1.6177\times10^{-5}$ m^2 s^{-1}, $D_{H_2/N_2}=8.1550\times10^{-5}$ m^2 s^{-1}, and $D_{H_2/CO_2}=6.8023\times10^{-5}$ m^2 s^{-1}.

The analytical model derived in Section Model Development and Theoretical Analysis allows us to calculate the hindrance factor α to predict how the solution for the uniform tube deviates from the solution for the conical tube. By means of Eq. 38 and the experimental dimensions stated in Table 1, we obtain a hindrance factor of $\alpha = 1.679$ saying that diffusion is approximately 68% slower in the conical tube. Here, it has to be noted that the average cross sections of the manufactured tubes are not identical (see Table 1). The comparability of the tubes, however, is given by the definition of α according to Eq. 38.

Comparison of model and experiment

In Figure 6, the predictively calculated temporal change of the molar fraction of each gas species in both bulbs is compared to the experimental results that are additionally provided in Tables A1–A3 in Appendix of this work. The molar fractions x_i are plotted vs. time t that is normalized with a factor regarding the geometric properties of the two-bulb diffusion cell. The analytical solution, Eq. 34, was evaluated in the eigenvalue space using the diffusivities at the equilibrium condition. Afterward, the physical compositions were computed using Eq. 37. Generally, it can be observed that the

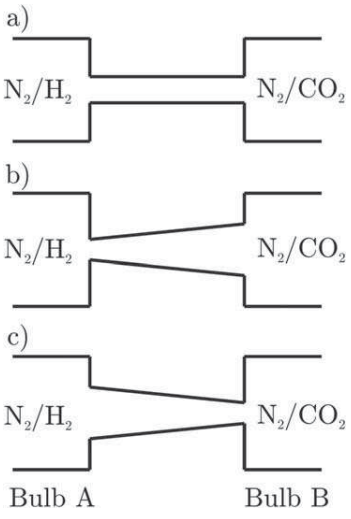

Figure 5. Different settings considered.

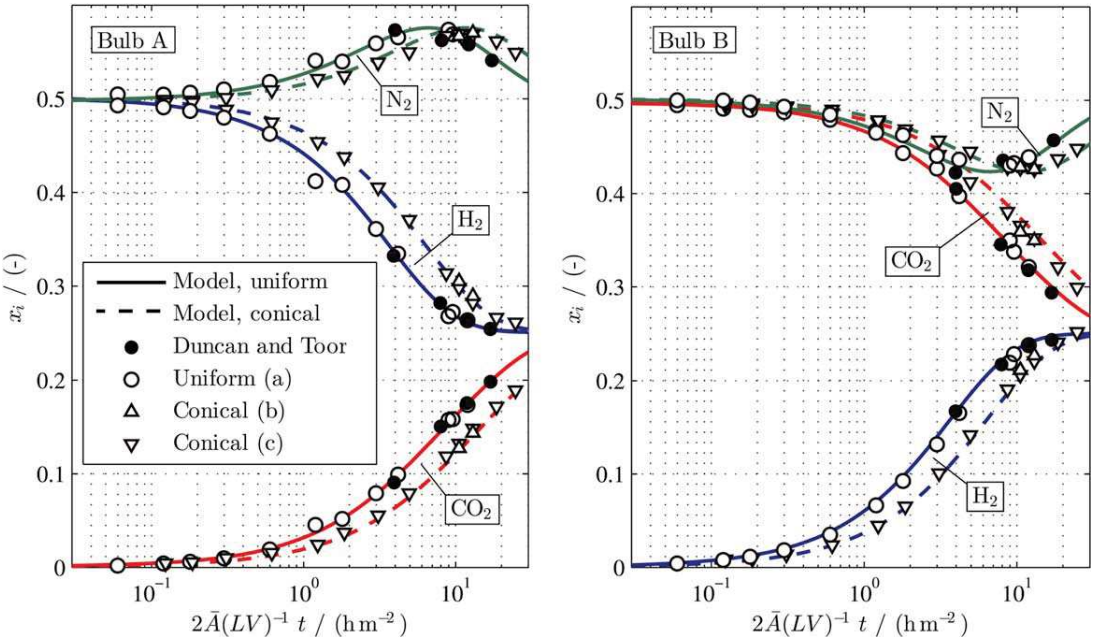

Figure 6. Comparison of analytical and experimental results for a uniform tube (solid lines, circles) and a conical tube (dashed lines, triangles) at 308.15 K and 0.1 MPa(a).

The molar fraction of nitrogen, hydrogen, and carbon dioxide is plotted vs. time that is normalized by the duct geometries and bulb volumes allowing also for a comparison with the results of Duncan and Toor.[11] Experiments on the conical tube were performed in both directions (see Figures 5b, c). The predictions were obtained using the model Eq. 34 and transformation from the eigenvalue space to the real space. Initial conditions for the calculations are given in Table A3 in Appendix. [Color figure can be viewed in the online issue, which is available at wileyonlinelibrary.com.]

diffusion of hydrogen and carbon dioxide follows Fick's law, that is, diffusion occurs from a high molar fraction to a lower molar fraction until equilibrium is reached. More interesting although, is the behavior for the diffusion of nitrogen that has the same molar fraction in both bulbs when the experiment starts. From $t = 0$, nitrogen diffuses from bulb B to bulb A although the gradient of molar fraction driving the diffusion is zero. Until the extremum is reached nitrogen diffusion occurs in direction of the increasing gradient which is contradictory to Fick's law. Finally, diffusion stops despite a large driving force. In literature, these effects are often referred to as osmotic diffusion, reverse diffusion, and diffusion barrier.[2,9]

Now, we focus the uniform tube that allows us to compare our analytical and experimental results to the data of Duncan and Toor.[11] As it can be seen in Figure 6, the solid curves are in excellent agreement to the filled circles that represent the experimental data of Duncan and Toor.[11] The experimental results obtained in this work are in very good agreement to the predictive calculations and to those of Duncan and Toor.[11] Here, it is worth noting that in their experiment the tube had a length of 85.9 mm, a diameter of 2.08 mm, and each bulb had a volume of 78 cm^3. Thus, we can show that the scaling factor $2A(LV)^{-1}$ allows to compare two-bulb diffusion cells with different geometrical properties. This is an important finding for future work in this field.

The dashed curves in Figure 6 are the predicted results for the slightly tapered tube with dimensions given in Table 1. As stated earlier, the average cross section of the cone is not identical to the cross section of the uniform tube. Hence, $2\bar{A}(LV)^{-1}$ is used for scaling t. The experimental results are given by the triangles whereby the 17 h and the 21 h experiments were performed for the diverging case (Δ, Figure 5b) and for the converging case (∇, Figure 5c). For the conditions considered here, the comparison indicates that the direction of the tapered tube does not affect the results as it is also analytically found in Section Model solution and analysis. All experimental results obtained on the conical tube are in excellent agreement to the developed model. This also demonstrates that the assumption of constant diffusivities is valid for the considered case. Consequently, the analytical solution of the presented model provides a valuable tool for most engineering purposes.

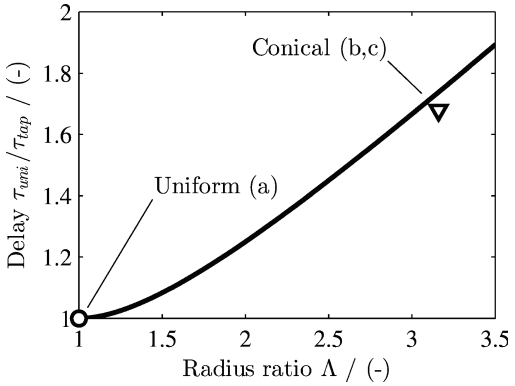

Figure 7. Delayed diffusion due to conicity. The curve is calculated according Eq. 39 with values given in Table 1.

The symbols, calculated according to Eq. 38, correspond to the hindrance factor ϰ scaling between the actual tube geometries.

Most interesting although is the comparison between the uniform and the tapered tube; the codiffusion and counterdiffusion of all species is significantly delayed by the conicity of the tapered tube (Figure 6). This becomes more obvious when using expression (39) to compute the relative delay $\alpha = \tau_{cone}/\tau_{uni}$ as a function of Λ, shown in Figure 7. The two points represent both test tubes that were used for the experiments whereby $\circ$ indicates the uniform tube with $\Lambda = 1$ and ∇ indicates the conical tube with $\Lambda = 3.16$. In case of this comparison, the diffusion in the conical tube is delayed by 68% that is experimentally confirmed by the data shown in Figure 6.

Consequently, the flux in a tapered duct is always lower compared to the one in a uniform duct with identical average cross section $\bar{A}$. Furthermore, this effect increases with increasing Λ whereby it seems to be indifferent whether $r^{(0)}$ or $r^{(L)}$ is larger.

Conclusions

The classical MSE are adapted for the prediction of ideal ternary diffusion in a two-bulb diffusion cell with a slightly conical tube. It is found that the temporal change of the molar fraction of each gaseous species is scaled by a simple factor $2A^{(0)}/(\Lambda LV)$ (Eq. 34) that includes all geometrical properties of the two-bulb diffusion cell. By means of that factor it is analytically shown that the direction in which the tube is assembled between the bulbs does not affect the result (Eq. 39).

To validate the derived model, a two-bulb diffusion cell is set up and the experiment of Duncan and Toor[11] is successfully reproduced using a tube with uniform cross section. In a next step, two-bulb diffusion experiments using a slightly conical tube are performed. The experimental results obtained on both geometries, uniform and slightly conical, are in excellent agreement to the analytical model. For the actual conditions, it is experimentally confirmed that the orientation of the conical tube (converging or diverging along z) does not affect the molar fraction of species at a certain instant of time.

Comparison between the uniform and the tapered tube shows that codiffusion and counterdiffusion of all species is significantly (68%) delayed by the conical geometry considered in this work. It is analytically found that this geometrical diffusion hindrance increases with the ratio of inlet to outlet cone radius. Consequently, for gaseous diffusion in "real" pores, that typically are somehow tapered, the transport limitation is even more serious than considered so far. Further investigation on process intensification, for example, gas separation and heterogeneous catalysis requires more accurate models and the taperedness of pores should be taken into account. Here, we want to emphasize the importance for the modeling of transport in fuel cells where the use of effective diffusion coefficients is state of the art.[3–6]

Finally, we emphasize that the strong diffusion hindrance for gas mixtures by nonuniform tubes is even present under standard pressure in macroscopic tubes and hence under negligible rarefaction. This is in contrast to the "diode effect" in pressure-driven flows that only occurs under rarefied conditions.[17–19] Further the "geometrical hindrance effect" for multicomponent gas diffusion described here is found to be independent of gradient orientation, whereas the "diode effect" is direction depended.

Future work includes the theoretical and experimental investigation of gaseous transport in tapered ducts under moderate rarefaction, as well as steady-state conditions.

Acknowledgments

The authors would like to thank Michael Birkner from the UFT mechanical workshop for his obliging assistance with the manufacturing of the experimental setup. The authors further acknowledge the input during the review process which let to significant improvement of the article. This work was financially supported by the German Research Foundation (DFG) through funding VE 808/1-1, and through the DFG Research Training Group GRK 1860 "Mirco-, meso-, and macroporous nonmetallic materials: Fundamentals and applications" (MIMENIMA).

Literature Cited

1. Bird RB, Stewart WE, Lightfoot EN. *Transport Phenomena*. New York: Wiley, 2007.
2. Taylor R, Krishna R. *Multicomponent Mass Transfer*. New York: Wiley, 1993.
3. Zhukovsky K, Zhukovskij VC. 3D model of oxygen-nitrogen transport in porous diffuser of hydrogen fuel element with polymer electrolyte. *Vestn Moskov Univ Ser 3 Fiz Astronom*. 2002;5:23–30..
4. Zhukovsky K. Three dimensional model of oxygen transport in a porous diffuser of a PEM fuel cell. *AIChE J*. 2003;49:3029–3036.
5. Zhukovsky K, Pozio A. Maximum current limitations of the PEM fuel cell with serpentine gas supply channels. *J Power Sources*. 2004;130:95–105.
6. Zhukovsky K. Modeling of the current limitations of PEFC. *AIChE J*. 2006;52:2356–2366.
7. Fick A. On liquid diffusion. *Philos Mag*. 1855;4:30–39.
8. Fick A. Über Diffusion. *Ann Phys*. 1855;170:59–86.
9. Krishna R, Wesselingh JA. The Maxwell-Stefan approach to mass transfer. *Chem Eng Sci*. 1997;52:861–911.
10. Bothe D. On the Maxwell-Stefan approach to multicomponent diffusion. In: Escher J, Guidotti P, Hieber M, Mucha P, Prüss JW, Shibata Y, Simonett G, Walker C, Zajaczkowski W, editors. *Parabolic Problems. Volume 80 of Progress in Nonlinear Differential Equations and Their Applications*. Basel: Springer Basel, 2011:81–93.
11. Duncan JB, Toor HL. An experimental study of three component gas diffusion. *AIChE J*. 1962;8:38–41.
12. Maxwell JC. On the dynamical theory of gases. *Philos Trans R Soc A*. 1866;157:49–88.
13. Stefan J. Über das Gleichgewicht und die Bewegung, insbesondere die Diffusion von Gasgemengen. *Sitzungsber Kaiserl Akad Wiss Wien*. 1871;63:63–124.
14. Lightfoot EN. *Transport Phenomena and Living Systems: Biomedical Aspects of Momentum and Mass Transport*. New York: Wiley, 1974.
15. Krishna R, Standart GL. A multicomponent film model incorporating a general matrix method of solution to the Maxwell-Stefan equations. *AIChE J*. 1976;22:383–389.
16. Kapteijn F, Bakker WJW, Zheng G, Poppe J, Mouljin JA. Permeation and separation of light hydrocarbons through a silicate-1 membrane: application of the generalized Maxwell-Stefan equations. *Chem Eng J*. 1995;57:145–153.
17. Veltzke T, Baune M, Thöming J. The contribution of diffusion to gas microflow: an experimental study. *Phys Fluids*. 2012;24:082004.
18. Veltzke T. *On Gaseous Microflows Under Isothermal Conditions. Ph.D. Thesis*. Bremen: University of Bremen, 2013.
19. Graur I, Veltzke T, Méolans J, Ho M, Thöming J. The gas flow diode effect: theoretical and experimental analysis of moderately rarefied gas flows through a microchannel with varying cross section. *Microfluid Nanofluid*. In press. DOI: 10.1007/s10404-014-1445-4.
20. Jacobs MH. *Diffusion Processes*. New York: Springer, 1967.
21. Zwanzig R. Diffusion past an entropy barrier. *J Phys Chem*. 1992; 92:3926–3930.
22. Berezhkovskii AM, Pustovoit MA, Bezrukov SM. Diffusion in a tube of varying cross section: numerical study of reduction to effective one-dimensional description. *J Chem Phys*. 2007;126:134706.

Appendix

Appendix provides the pictures from which the tube inlet cross sections were obtained. Further, all raw data of the two-bulb diffusion experiments are tabulated.

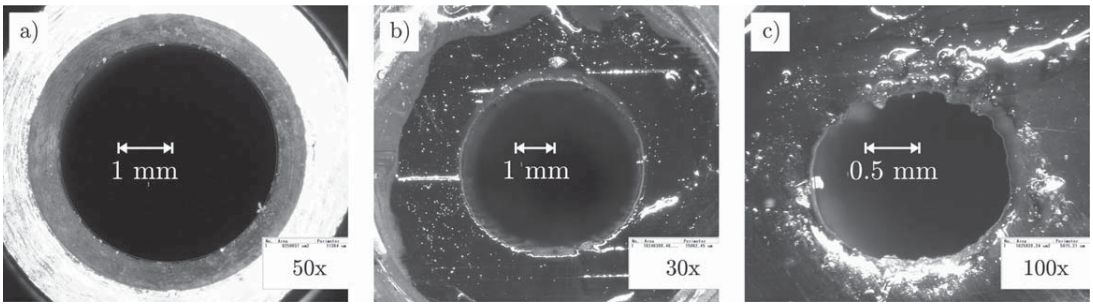

Figure A1. Inlet cross-sectional areas of investigated tubes measured with a digital light microscope.

In case of the steel tube with uniform cross section (a) a circle was approximated to the contour. The areas of the large entrance (b) and the small entrance (c) of the conical tube manufactured by stereo-lithography were contoured by means of a polygon. Results are stated in Table 1.

Table A1. Experimental Results Obtained on the Uniform Tube (Figure 5a) at 308.15 K and 0.1 MPa(a)

Time	Bulb A			Bulb B		
t (h)	x_{CO_2}	x_{N_2}	x_{H_2}	x_{CO_2}	x_{N_2}	x_{H_2}
0.1	0.0020	0.5047	0.4931	0.4948	0.4999	0.0043
0.2	0.0042	0.5046	0.4910	0.4911	0.4998	0.0079
0.3	0.0060	0.5067	0.4871	0.4898	0.4976	0.0115
0.5	0.0097	0.5102	0.4800	0.4874	0.4933	0.0185
1	0.0191	0.5180	0.4627	0.4792	0.4847	0.0351
2	0.0455	0.5408	0.4121	0.4677	0.4653	0.0665
3	0.0517	0.5398	0.4082	0.4434	0.4628	0.0927
5	0.0793	0.5593	0.3610	0.4269	0.4405	0.1320
7	0.0992	0.5658	0.3346	0.3973	0.4364	0.1654
15	0.1575	0.5738	0.2678	0.3498	0.4300	0.2193
16	0.1584	0.5689	0.2723	0.3378	0.4328	0.2286
20	0.1735	0.5622	0.2635	0.3214	0.4390	0.2382

Table A2. Experimental Results Obtained on the Conical Tube According to Figure 5b at 308.15 K and 0.1 MPa(a)

Time	Bulb A			Bulb B		
t (h)	x_{CO_2}	x_{N_2}	x_{H_2}	x_{CO_2}	x_{N_2}	x_{H_2}
17	0.3592	0.4287	0.2115	0.1274	0.5671	0.3052
21	0.3499	0.4261	0.2272	0.1437	0.5706	0.2892

Table A3. Experimental Results Obtained on the Conical Tube According to Figure 5c at 308.15 K and 0.1 MPa(a)

Time	Bulb A			Bulb B		
t (h)	x_{CO_2}	x_{N_2}	x_{H_2}	x_{CO_2}	x_{N_2}	x_{H_2}
0	0.0003†	0.4978†	0.5012†	0.4963†	0.5016†	0.0006†
0.2	0.0043	0.4990	0.4964	0.4942	0.4969	0.0085
0.3	0.0054	0.4982	0.4961	0.4941	0.4967	0.0089
0.5	0.0099	0.5012	0.4887	0.4935	0.4924	0.0139
1	0.0155	0.5092	0.4749	0.4902	0.4861	0.0237
2	0.0242	0.5214	0.4539	0.4761	0.4786	0.0448
3	0.0373	0.5245	0.4377	0.4654	0.4690	0.0654
5	0.0555	0.5388	0.4053	0.4416	0.4571	0.1009
8	0.0792	0.5499	0.3706	0.4124	0.4451	0.1418
14	0.1185	0.5672	0.3137	0.3804	0.4284	0.1907
17	0.1322	0.5693	0.2982	0.3656	0.4277	0.2062
21	0.1483	0.5691	0.2822	0.3524	0.4262	0.2209
30	0.1718	0.5617	0.2661	0.3212	0.4370	0.2412
40	0.1891	0.5492	0.2611	0.2993	0.4482	0.2518

Results indicated with † are the initial values used for calculations.

Manuscript received July 22, 2014, and revision received Dec. 2, 2014.